Princeton Plasma Physics Laboratory

PPPL- 4879

PPPL- 4879

# Boundary Perturbations Coupled to Core 3/2 Tearing Modes on the DIII-D Tokamak

B.J. Tobias, et. al.

May, 2013

PPPL PRINCETON PLASMA PHYSICS LABORATORY

Prepared for the U.S. Department of Energy under Contract DE-AC02-09CH11466.

# Princeton Plasma Physics Laboratory
# Report Disclaimers

---

## Full Legal Disclaimer



## Trademark Disclaimer



---

# PPPL Report Availability

## Princeton Plasma Physics Laboratory:

http://www.pppl.gov/techreports.cfm

## Office of Scientific and Technical Information (OSTI):

http://www.osti.gov/bridge

---

**Related Links:**

**U.S. Department of Energy**

**Office of Scientific and Technical Information**

**Fusion Links**

# Boundary perturbations coupled to core 3/2 tearing modes on the DIII-D tokamak

B. Tobias[1], L. Yu[2], C.W. Domier[2], N.C. Luhmann, Jr.[2], M.E. Austin[3], C. Paz-Soldan[4], A.D. Turnbull[5], I.G.J. Classen[6] and the DIII-D team

[1]*Princeton Plasma Physics Laboratory, Princeton, NJ, USA*

[2]*University of California at Davis, Davis, CA, USA*

[3]*Universtiy of Texas at Austin, Austin, TX, USA*

[4]*Oak Ridge Institute for Science and Education, Oak Ridge, TN, USA*

[5]*General Atomics, CA, USA*

[6]*FOM-Institute DIFFER, Nieuwegein, The Netherlands*

e-mail: bjtobias@pppl.gov

**Abstract.** High confinement (H-mode) discharges on the DIII-D tokamak are routinely subject to the formation of long-lived, non-disruptive magnetic islands that degrade confinement and limit fusion performance. Simultaneous, 2D measurement of electron temperature fluctuations in core and edge regions allows for reconstruction of the radially resolved poloidal mode number spectrum and phase of the global plasma response associated with these modes. Coherent, $n$=2 excursions of the plasma boundary are found to be the result of coupling to an $n$=2, kink-like mode which arises locked in phase to the 3/2 island chain. This nonlinear coupling dictates the relative phase of the displacement at the boundary with respect to the tearing mode. This unambiguous phase relationship, for which no counter-examples have been observed, is presented as a test for modeling of the perturbed fields to be expected outside the confined plasma.

PACS Nos.: 52.35.Mw, 52.35.Py, 52.55.Fa

## 1. Introduction

Though the modern tokamak remains a nominally axisymmetric configuration, understanding non-axisymmetric features of the plasma response to both applied (external) magnetic fields and spontaneous, internal MHD remains an important issue. 3D resonant magnetic perturbations produced by coils outside the plasma show great potential for mitigating or suppressing large Type-I edge localized modes (ELMs) [1-3], modifying resistive wall mode (RWM) stability [4, 5], and controlling internal MHD [6-8]. And the interaction between applied fields and internal MHD is used routinely as a metric in error field correction techniques [9, 10]. But, the complete picture as to what specific resonances are most important in these processes remains somewhat unclear [11-13]. Changes in MHD stability follow from a plasma response that is the product of competition between field penetration and screening by plasma currents [14-16]. Amplification of the field may contribute to 3D shaping of the plasma, access to non-axisymmetric equilibrium states, and a 3D displacement of the plasma boundary. Penetration of an applied field may induce magnetic islands, having either beneficial or deleterious results. The problem is highly nonlinear, and there remains a great deal of controversy over which modeling methods predict the appropriate non-axisymmetric state. Various tools that are currently considered state of the art often yield qualitatively different solutions [17]. With these considerations in mind, it becomes painfully clear why enhancing our understanding of processes at play in 3D tokamak operation and validating the numerical tools available for predicting

their influence is critical and timely in preparation for the next step in fusion science: the operation of a burning plasma experiment on the scale of ITER. However, even simple diagnosis of 3D field quantities in existing experiments is non-trivial and complicated by many factors.

Having a limited view of the plasma from fixed toroidal locations, it is necessary to rotate the 3D perturbation past the field of view of each diagnostic for a complete picture. Due to intrinsic error fields, the physical limitations of magnetic perturbation coils, and the fact that non-inductive sources of heating and current drive are fixed in their respective positions, this practice inevitably introduces further complications. Discharges with rotating applied magnetic perturbation fields are often subject to modulation of global plasma parameters, and limited diagnostic access makes the removal of these contributions to the measurement daunting [18]. Keeping in mind that our goal is to uncover constraints for the nonlinear relationships between non-axisymmetric magnetic fields in vacuum regions outside the confined plasma, nominally helical excursions of the plasma boundary, and non-axisymmetric modes within the core plasma, it is sensible to first seek these constraints for spontaneous plasma responses that are inherently coherent, rotate with the plasma fluid at a frequency which is separable from all global variations of the plasma equilibrium, and are thereby readily diagnosed by existing systems. This more tractable approach will then provide guidance to modeling the physics that preclude solving the inverse problem of how to prescribe an artificial vacuum field that influences the plasma in a predictable way.

We observe that core eigenmodes, resulting from field line tearing and the formation of magnetic islands, couple strongly to external magnetic coils and are routinely observed to induce a localized displacement of the plasma boundary. These internal MHD are inherently of interest for the stability of current and future tokamak devices [19] due to their proclivity to lock, resulting in disruption and the loss of plasma confinement [20]. Therefore, diagnosing them, constraining models for their coupling to other modes and fields in vacuum, and improving the effectiveness of techniques for their control represents an important contribution to fusion science in its own right. It may eventually lead to improved schemes for applying torque to internal MHD that have modest toroidal rotation in the laboratory frame [7, 21], or detecting the absolute phase of rotating magnetic islands from external magnetic measurement alone. Improved island detection would have significant impact on the efficiency of neoclassical tearing mode (NTM) suppression using localized RF current drive [19, 22-24]. In this work, we provide unambiguous constraints on the interaction between core $m$=3, $n$=2 magnetic islands and observable displacements of the plasma boundary, revealing that they are the product of coupling to a kink-like plasma response. This observation exposes a shortcoming in theory, namely that kink mode stability cannot be evaluated in the presence of a prescribed tearing mode.

In this paper, the diagnosis of 3D perturbations both internal and external to the tokamak plasma, coupled through the nonlinear evolution of a global kink mode, is presented as a constraint and motivation for modeling efforts. In Section 2, the experimental method is described both in terms of the discharge parameters and

the analysis techniques applied. Particular focus is placed on the interpretation of edge measurements made by ECE-Imaging, as this analysis requires attention to subtleties unique to this region of the plasma. Section 3 presents the orientation of flux surface displacements throughout the imaging window, revealing an interesting phase relationship between the internal MHD and the displacement of the plasma boundary. An axisymmetric equilibrium reconstruction, averaged over many periods of the 3D perturbation, is utilized in Section 4 to produce the radially resolved poloidal mode number spectrum of the plasma response. This technique analysis exposes regions of pitch-resonant response, as well as regions that are kink-like and are not similar in mode number to the local magnetic field line winding number. Section 5 concludes with a summary of the most pertinent observations and a discussion of their implications for fusion science and theoretical modeling.

## 2. Simultaneous core and edge imaging of ECE

### *2.1. Discharge parameters and general MHD behavior*

For this study, a sampling of diverted, H-mode discharges from the DIII-D tokamak that meet the following criteria were chosen: 1) plasma density and magnetic field are such that core and edge regions remain accessible to ECE diagnostics and not in cutoff, 2) they exhibit spontaneous formation of long-lived, non-disruptive 3/2 tearing modes, 3) $q_{\min}$ remains marginally above unity such that there are no sawteeth, 4) there are no detectable 2/1 tearing modes, and 5) a steep pressure pedestal forms, leading to regular Type-I ELMs. Among these discharges, plasma shape and toroidal field were held constant while injected neutral beam power from was varied from approximately 6 to 10 MW. Plasma current varies from 1.2 to 1.7 MA. In the interest of disclosure, we note that many of the discharges analyzed included static or slowly rotating $n$=2 magnetic perturbations from the so-called I-coil. However, times with modified ELM behavior have been excluded from the dataset (along with all instances of observed changes in rotation due to the applied field or unstable 2/1 islands). Therefore, any applied magnetic perturbation field constitutes a non-axisymmetry that is stationary in the laboratory frame and does not appear to interact with the modes of interest, which are rotating toroidally at approximately 15 kHz.

A dual-array ECE-Imaging system installed on the DIII-D tokamak makes use of partially separate focusing optics so as to enable imaging of two radially separated plasma regions at the same toroidal angle [25]. Aligning this system such that one array of 160 channels (8 radial x 20 vertical) views a region encompassing the $q$=3/2 rational flux surface and the other (also 160 channels) images the plasma edge, the ECE spectrum

may be obtained, in 2D, for both regions simultaneously. The Fourier transformed time domain signals obtained by each of these 320 channels reveal a coherent oscillation, isolated in frequency but distributed across multiple core and edge channels. Digital finite impulse response (FIR) signal post-processing and fast Fourier transform (FFT) based eigenmode analysis techniques allow these coherent oscillations to be isolated and imaged without the corruption of unrelated, transient mode activity or diagnostic artifacts that may exist at other, disparate frequencies. The result is 2D data, localized in ECE frequency and real space, as shown in Figure 1. It accurately represents the coherent mode activity in a narrow frequency band (~1 kHz). Because ECE-Imaging data is collected from points on a nearly uniform grid of vertical elevation, $z$, and ECE frequency, $\omega_{ce}$ (a function of local magnetic field modulus), it is finely spaced in a flux conserving coordinate system. Each data point often has a unique coordinate in $\varrho$ and $\theta$. This allows for the reconstruction of perturbation eigenfunctions with high resolution in $\varrho$-space and serves as the basis for more detailed analysis.

The 1D ECE radiometer [26], having a line of sight near the midplane but separated toroidally from the ECE-Imaging system by 190°, has radial coverage overlapping both regions of ECE-Imaging measurement, albeit with a different radial resolution. This makes it useful for monitoring the intervening gaps in ECE-Imaging data. Radially resolved FFT spectra from the 1D radiometer provide radially continuous coverage that can be used to diagnose the presence of other modes that may complicate the analysis or violate the controls of this experiment (e.g. 2/1 tearing modes). Plotting this data along with the toroidal fluid rotation as measured by charge-exchange/recombination spectroscopy (CER) also helps to identify the modes of interest and validate our

interpretation of their nature. Figure 2 a) shows this data for shot 148753 at 3136 ms. External measurements from the toroidally distributed Mirnov coil array confirm that the oscillations observed at 29.5 kHz are of an $n$=2 toroidal phase distribution. A sharp phase transition in the radial eigenfunction of the core oscillation near $q$=3/2 ($\varrho$=0.48) corresponds to the center of the magnetic island chain. At this radius, the frequency of the oscillation is shifted 4 kHz in the ion diamagnetic direction from the CER fluid rotation measurement, as one would expect due to the finite rotation of the NTM near the threshold of stabilizing polarization currents [27]. The kink mode that is destabilized at smaller minor radii is in the rest frame of the plasma at $R$=1.965 m ($\varrho$=0.35). Internal kink modes of this kind, stationary in the plasma rest frame, are routinely observed in a variety of other discharges [28]. The response at large minor radii, however, is far from resonant with the frequency of toroidal rotation. It is instead coupled to the frequency of the mode activity in the core. Interestingly, the eigenfunction is exceedingly weak at intervening radii in the vicinity of $\varrho$=0.65, and there is no detectable $n$=1 mode activity. This of course presents a mystery as to the nature of the coupling between the MHD in core and edge regions, if they are to be conceived as separate modes, since the coherent perturbation eigenfunction is discontinuous.

Mirnov array data has been used extensively to obtain the toroidal phase distribution of the coherent oscillation and aid in identification of the internal modes. However, we do not find the amplitude of the $n$=2 oscillation detected by the Mirnov coils to be an indicator of island width. The amplitude of the $n$=2 oscillation as detected by a Mirnov coil located at the midplane, near the toroidal location of the 1D radiometer, is plotted vs. the coherent amplitude of the ECE response in the region of the core kink mode ($\varrho$=0.35)

in Figure 3 a). In shot #148753, a linear correlation of 0.78 is observed between these diagnostic signals over the interval of 15 to 35 kHz and 2500 to 3800 ms. No such correlation is observed in Figure 3 b), where the island width is estimated from ECE data for the same times. These estimates are limited by the resolution of the 1D radiometer, which has a channel spacing of approximately 2.5 cm in this region.

*2.2. Interpretation of images from the plasma edge*

Interpretation of ECE-Images from the core plasma is straightforward. The emission perpendicular to magnetic field lines at the second ECE harmonic and in x-mode polarization originating from this region is optically thick, meaning that the source of emission is localized and the observed intensity is proportional to the local electron temperature. Interpreting the coherent image as a fluctuation of the electron temperature profile in response to the displacement of magnetic flux surfaces is valid and well documented, particularly with respect to diagnosing the topology of magnetic islands consistently with thermal transport about the island separatrix [29-32]. However, one must be more careful when attempting to interpret images where the measured ECE frequency spans the cold plasma resonances of the plasma edge [33].

The primary complication that arises when imaging the plasma edge concerns the rapid transition from an optically thick region to tenuous, optically thin plasma. Relativistically downshifted emission from inside the LCFS passes through regions of weak reabsorption outside the LCFS, and anomalously high radiation temperatures are recorded at frequencies below the cold plasma resonance of this boundary. Radiation temperature profiles that exemplify this so-called “shine-through” effect, which arises due to the presence of a steep pressure pedestal near the plasma edge, may be found in

refs. [33-35]. This effect is commonplace during H-mode operation on DIII-D, and because the shine-through radiation is non-local, the observed intensity in this portion of the spectrum may either increase or decrease in response to a displacement of the plasma boundary, depending on a complicated interplay between emission and absorption along the diagnostic line of sight. Therefore, it is necessary to model the ECE radiation transport on a case-by-case basis using electron temperature and density profiles consistent with independent measurement. By this method, one may self-consistently locate the edge of the plasma in frequency space, empirically determine the optical thickness as a function of frequency, and more accurately remap the diagnostic data from frequency space to the time averaged positions of flux surfaces in real space.

A simplified computational approach for modeling ECE radiation transport has been quantitatively validated for the diagnostic configuration and typical H-mode pedestal characteristics relevant to DIII-D, and it produces easily recognizable qualitative features that allow the interpretation of ECE-Imaging data to be accomplished simply and consistently with intuition [33]. The most recognizable of these features is an alternating phase structure in fluctuating radiation temperature, $\delta T_{RAD} = T_{RAD} - \langle T_{RAD} \rangle$. For an example of this response in the ECE spectrum we refer to Figure 1 c). Crossing the last closed flux surface (LCFS), the phase of the coherent perturbation inverts suddenly, and then changes back again. The outermost region consists primarily of relativistically downshifted emission propagating along an optically thin path toward the diagnostic, and is correlated to pressure perturbations inside optically thick regions of the plasma. The central, phase inverted band of the ECE-Image has characteristics that are sensitive to the steepness of the pedestal and responds in a fashion anti-correlated to pressure

perturbations near the plasma edge. Its presence improves the confidence with which the plasma boundary may be located in frequency space and the ECE spectrum mapped to real coordinates.

The inner region of the ECE-Image represents an effectively optically thick measurement in that it is correlated to a localized change in electron temperature, $\delta T_e = -\xi \bullet \nabla T_e$. Hence, it may be used to diagnose the phase and relative amplitude of the plasma displacement, $\xi$. When properly mapped to flux surfaces inside the plasma, the 2D phase variation provides the wavelength of the perturbation on these flux surfaces. This may then be converted to a poloidal mode number by fitting the wavelength to appropriately selected basis dictated by an equilibrium reconstruction of the discharge [33, 36]. Reporting the results as a function of plasma minor radius defines the radially resolved mode number spectrum of the plasma response. As a corollary, the absolute phase of this response may be compared to other time varying diagnostic signals when sampled at the same rate and subjected to equivalent time delays to account for analog and/or digital signal processing, such as frequency filtering. The results of this analysis are presented in the following sections.

## 3. Coupled phase of core and edge responses and the orientations of radial flux surface displacements

By simultaneously imaging core and edge regions of the discharge with multiple arrays of the same diagnostic system, the relative phase in these regions may be compared in exactly the same manner as if they had been diagnosed by a continuous, 2D image. It has been observed that the amplitude of the ECE response at the edge of the plasma, and the amplitude of the $n$=2 response of the Mirnov array, are closely related to the amplitude of an ECE response in the core of the plasma, nearly 10 cm inside the $q$=3/2 radius. Meanwhile, by applying a model for helical perturbations in $T_e$ due to island formation developed by Fitzpatrick in ref. [29], we track the island width and find no correlation. It then follows that diagnosing characteristics of the island chain (including the absolute phase of the island x and o-points) from external, magnetic measurement requires a model for the fields in vacuum that accounts for the secondary, kink-like mode and produces a displacement of the boundary that is of the proper sign. For the discharges described in this work, that displacement is in phase with the kink-like displacement deep in the plasma core, but opposes the deformation of flux surfaces near the outer separatrix of the island chain.

The fitted radial eigenfunction of the plasma response is plotted in Figure 4 a), along with the phase of the coherent ECE-Imaging signal along lines of sight at different vertical elevations. Because the ECE-Imaging view is nominally bi-rectangular and composed of 320 regularly spaced channels, the resolution in flux coordinate space is much greater than possible along any single line of sight. This enhanced resolution in $\varrho$ provided by the 2D diagnostic distinguishes the composite eigenfunction of a coupled

tearing mode and internal kink mode from the simpler eigenfunction that would result from a large, asymmetric island chain, such as that described in ref. [30]. The absolute peak of the eigenfunction (which corresponds to the inner extreme of the island separatrix) and the peak of the internal kink mode are distinct, separated by a small dip in the eigenfunction near $\varrho$=0.4, allowing key parameters of the two modes to be differentiated and independently diagnosed. The positions of peaks in the eigenfunction that define the island width [29] are relatively symmetric about the rational surface. They indicate that the island width varies from 2 to 8 cm over the discharges analyzed and is 5.5 cm at the time shown. This determination is independent of the asymmetry in the amplitude of the eigenfunction peaks, which we deem to be primarily the result of the superposition of the internal kink.

For the diagnostic arrangement shown, channels of the high field side array near the midplane observe only the inner half of the island chain. However, at an elevation of several cm they sample points on either side of the rational surface and reflect the phase inversion characteristic of periodic temperature profile flattening due to island formation. Points from the low field side array viewing regions inside the LCFS are selected for comparison to the core eigenfunction. The phase of these measurements is in agreement with the inner portion of the island (and the core kink mode), but they are in anti-phase with respect to the portion of the island outside the rational surface. Furthermore, one may note from this data that eigenmode phase in the core varies along each of the diagnostic lines of sight, which are nominally aligned to the tokamak major radius. This variation is subdued in the low field side data that encompasses the plasma edge. Figure 4 b) illustrates the orientation of displaced flux surfaces, as determined from ECE-Imaging

data and using well-validated models for the underlying ideal displacements [31, 33, 37]. Following a flux surface around the tokamak at elevations near the midplane by varying the toroidal angle, the plasma boundary is displaced inward, toward island o-points, and outward, away from island x-points.

This result is striking in that it is in contradiction to the presumption that displacements at the boundary are the result of unidirectional displacements originating in the core plasma. In many discharges where 2/1 islands are destabilized at radii between the 3/2 island chain and the plasma edge, the preferential toroidal phase relationship between the 3/2 and 2/1 islands results in dramatic deformation of the 3/2 island chain and accounts for the phase reversal of the displacement at the boundary with respect to the island separatrix (c.f. Figure 4, ref. [38]). However, the dataset used here purposefully excludes discharges with 2/1 tearing mode activity, the 3/2 island chain is not distorted, and there is no evidence of other magnetic islands in this region, such as 4/2 modes. Islands too small to modify thermal transport [29, 32], hence having no signature in ECE data, cannot be excluded, but we find it unlikely that such small, weakly driven islands could be responsible for such a robust and general result. The amplitude of the perturbation falls below the detectable level between the 3/2 surface and the plasma boundary, and as will be discussed in the next section, responses in core and edge regions are very different with respect to their dominant poloidal mode number.

## 4. Radially resolved poloidal mode number spectra of spontaneous plasma non-axisymmetry

Toroidal mode number, or *n*-number, has been constrained by Mirnov coil array data, and because the response observed by ECE diagnostics is coherent at the Mirnov frequency, it is taken to be a constant. The poloidal mode number, or *m*-number spectrum is evaluated by fitting 2D ECE-Imaging data to basis functions of the form $\xi_m \sim e^{i(\theta_s m+\alpha)}$, where $\theta_s$ is the poloidal angle in a straight field line coordinate system where $d\theta_s/d\zeta = \mathbf{B}\bullet\hat{\theta}_s/\mathbf{B}\bullet\hat{\zeta} = \iota(\rho)$, and $\alpha$ is the absolute phase of the perturbation with respect to the FFT window. The rotational transform, $\iota$, is defined as a function of radial flux coordinate, $\varrho$, and $\zeta$ is the toroidal angle. In our analysis, the poloidal mode number, $m$, is not constrained to integer values. Rather, sub-integer values are permitted as dominant *m*-numbers in order to reflect the competition of multiple integer modes, which when simultaneously excited produce a ballooning eigenfunction due to regions of constructive and destructive interference. This approach follows from the well-known trigonometric identity, $\cos(\alpha)+\cos(\beta)=\cos\left(\frac{\alpha+\beta}{2}\right)\cos\left(\frac{\alpha-\beta}{2}\right)$, where the final term represents a slowly varying, or for our purposes ballooning, envelope function that satisfies periodic boundary conditions. The radially resolved data that results from this analysis is readily compared to the rotational transform, or equivalently the *q*-profile, and multiples thereof. It distinguishes field line pitch resonant activity from kinking or non-resonant ballooning behavior.

The fitted poloidal mode number spectrum of coherent mode activity throughout the plasma, observed at the frequency of *n*=2 oscillations detected by the Mirnov coil array,

is presented in Figure 5 a). As expected, the observed perturbation is found to be pitch resonant at the radius where $q$=3/2, as determined by EFIT reconstruction constrained by motional Stark effect (MSE) data and kinetic pressure profiles. Over the core radii observed by ECE-Imaging, the mode retains a dominantly $m$=3 nature, making it super-resonant to the $m = 2q$ curve at smaller minor radii, and sub-resonant at those larger minor radii observed up to approximately $\varrho$=0.55. No poloidal mode numbers are obtained in the region between the two ECE-Imaging arrays, where the coherent response is generally weak or indiscernible. However, near the edge of the plasma, in a region of optically thick measurement extending from $\varrho$=0.8 to 0.95, mode numbers approximating $m = (n+1)q$ (in our discharges $3q$) are observed. The fitted mode number trends upward approaching the LCFS, and a range of closely spaced harmonics indicate a ballooning-like eigenfunction. The resolution of this analysis is more than adequate to confirm, unambiguously, that the poloidal mode number of the boundary displacement is not similar to that of the coupled, internal island structure, and not locally pitch-resonant at optically thick radii $\varrho$<0.95.

It is interesting to note that there is a great deal of empirical evidence suggesting that a spectrum of poloidal harmonics near $m = (n+1)q$ constitutes a characteristic eigenmode of the plasma response. Previous studies using the MARS-F code [39] illustrate that, for low toroidal mode numbers ($n \leq 3$), poloidal mode numbers larger than those in pitch resonance with the equilibrium are excited at the same frequency as external perturbations. This result has been compared to experiment on DIII-D [14] using external magnetic diagnostics. Furthermore, though the amplitude of the excitation

varies, the relative position of the kink harmonic band observed has been shown to be relatively insensitive to resistivity, plasma $\beta$, and rotation [40].

Figure 5 b) shows an alternative decomposition obtained by fitting to the new set of basis functions $\xi_m \sim e^{i(\theta m+\alpha)}$, where $\theta$ in this case is the simple polar angle in the poloidal plane. This spectrum may be thought of as the normalized poloidal wavenumber of the mode within the diagnostic view, as it is approximated by $m \approx k * 2\pi r$ and may easily be transformed to a physical wavelength with units of $m^{-1}$. The ratio $d\theta_s/d\zeta$ being proportional to the rotational transform, $\iota$, in a straight-field line coordinate system, the large aspect ratio limit ($d\zeta \rightarrow dz$) of the transformation from polar angle to straight-field line poloidal angle, $d\theta/d\theta_s$, is simply $q$. Therefore, pitch-resonance is approximated by an intersection of the mode number with the $q$-profile, as seen in the decomposition of the core response near a radius of $\varrho$=0.5.

The normalized wavenumbers describing the core response decrease with radius, reaffirming our earlier observation that the mode is aligned in this region to flux conserving coordinates and that the poloidal wavelength at outboard radii increases faster than the geometric arc length (the inverse would be true at inboard radii). This trend continues up to the point of pitch resonance, which is the center of the magnetic island chain. Normalized wavenumbers beyond this radius, however, increase proportionally with $\varrho$, and the physical poloidal wavelength of the mode near the outboard midplane remains nearly constant from the radius of pitch resonance outward. This suggests, in keeping with the data shown in Figure 4, that the total plasma response is aligned along a coordinate not orthogonal to the straight field-line poloidal and toroidal unit vectors, but

rather more nearly aligned to major radius. As a consequence, the mode at large radii resembles an outward, shock-like displacement.

In Figure 5 c), a 2D reconstruction of the eigenmode structure in poloidal cross-section is shown. This reconstruction follows directly from the poloidal mode number decomposition as it is simply the basis functions best fit to the ECE-Imaging data plotted in 2D over the axisymmetric plasma equilibrium. It is reasonable to assume that flux conserving coordinates are most appropriate to describe the eigenmode structure, and so basis functions periodic in this coordinate system are used. This choice for the set of basis functions, as opposed to infinitely many other orthogonal vector spaces in which the available data may be equally well described, produces complicated, fine structure both near the crown of the discharge and in the divertor region. These regions are unconstrained by the data, as there are no imaging diagnostics presently available that provide adequate spatial and temporal resolution there. For this reason, we note that it remains impossible to independently verify that we have chosen the most appropriate set of basis functions, or that our extrapolation of the global eigenfunction is a correct description of the plasma response. It remains a hypothesis based on limited 2D data and the reasonable assumption that the eigenmode has structure aligned everywhere to the magnetic topology.

## 5. Summary and Discussion

In an effort to better understand the nature of non-axisymmetric, helical displacements near the plasma boundary, we have applied 2D ECE-Imaging techniques to a series of discharges in which a coherent perturbation of the H-mode pedestal arises as a result of nonlinear coupling to a long-lived, non-disruptive 3/2 tearing mode. This has produced a new observation that may aid in testing the validity of numerical models. Namely, the boundary perturbation, and the fields in vacuum diagnosed by Mirnov coil array, are correlated to the amplitude of a secondary, kink-like mode, which is locked in toroidal phase with the rotating 3/2 tearing mode. We speculate that this is a general result, and that non-linear coupling to kink-like eigenfunctions dominates the coupling of internal magnetic islands to fields in vacuum, outside the confined plasma.

We continue to seek a model that properly represents the global, kink-like response of the plasma in the presence of persistent magnetic islands. We reject simple models that describe the plasma response at the boundary as merely a smooth continuation of the core eigenfunction. For the following reason, such a description is not applicable to our data: at elevations near the midplane, both the amplitude and phase of the boundary response are correlated to those of the internal kink, resulting in a flux surface displacement that reverses between the island separatrix and the plasma edge. ECE data reveals no intermediate island chains or distortions of 3/2 islands that would trivialize this observation or diminish its generality. Furthermore, we observe that the poloidal mode number of the perturbation near the edge is not similar to that of the core island, but varies in a manner similar to what is routinely observed in modeling the linear, ideal plasma response to external magnetic perturbations. This suggests that the internal

perturbation may provide a similar trigger, exciting a characteristic eigenmode by similar processes.

Modeling this case will surely have practical implications for fusion science, particularly in the area of MHD sensing and control for the stable operation of advanced tokamak scenarios. The phase relationship observed between the displacement of the boundary and the island chain within the core suggests that a more complete model for the global plasma response is required before tearing mode island phase may be routinely and confidently determined by external magnetic measurement, such as by Mirnov coil arrays. This consideration, of course, adds complication to the path toward the most efficient schemes for tearing mode suppression and disruption avoidance, such as pulsed ECCD.

Toward the goal of generating a prescribed non-axisymmetric plasma response or controlling the stability of core MHD through the application of RMP fields, diagnosing a spontaneous, global eigenfunction represents a very small step along an arduous path. It remains unclear as to what extent the observed processes are reciprocal, and whether or not the external field spontaneously generated by a tearing mode corresponds to the most resonant field one would apply in order to influence said mode. There are inherent difficulties associated with generating an RMP field that is sufficiently close to stationary in the plasma frame, and yet it is well-known that plasma rotation has a significant impact on the plasma response [15, 41]. Furthermore, modeling suggests that applying even a relatively small magnetic perturbation ($10^{-3}$ relative to $B_T$) results in a breakdown of linear theory and a departure of the eigenfunction from that obtained by perturbative methods

[17]. Nonetheless, we report our findings with the hope that they find application in testing solutions for the relevant and most tractable aspects of this daunting challenge.

**ACKNOWLEDGMENTS**

The authors would like to thank W.A. Cooper, N.M. Ferraro, R.J. La Haye, S.C. Jardin, E.A. Lazarus, and A. Welander for their insights in discussion of this work. Work supported by U.S. DOE under DE-AC02-09CH11466, DE-FG02-99ER54531 and DE-FG03-97ER54415.

**References**


[1] K. Burrell *et al.*, Plasma Physics and Controlled Fusion **47**, B37 (2005).
[2] T. Evans *et al.*, Nuclear fusion **48**, 024002 (2008).
[3] W. Suttrop *et al.*, Physical Review Letters **106**, 225004 (2011).
[4] M. Baruzzo *et al.*, Nuclear fusion **52**, 103001 (2012).
[5] L. Piron *et al.*, Plasma Physics and Controlled Fusion **53**, 084004 (2011).
[6] R. Buttery *et al.*, Nuclear fusion **51**, 073016 (2011).
[7] F. Volpe *et al.*, Physics of Plasmas **16**, 102502 (2009).
[8] T. Hender *et al.*, Nuclear fusion **32**, 2091 (2002).
[9] J. Scoville, and R. La Haye, Nuclear fusion **43**, 250 (2003).
[10] J. K. Park *et al.*, Nuclear fusion **48**, 045006 (2008).
[11] M. Tokar *et al.*, Nuclear fusion **48**, 024006 (2008).
[12] M. Fenstermacher *et al.*, Physics of Plasmas **15**, 056122 (2008).
[13] O. Schmitz *et al.*, Physical Review Letters **103**, 165005 (2009).
[14] M. Lanctot *et al.*, Physics of Plasmas **18**, 056121 (2011).
[15] N. Ferraro, Physics of Plasmas **19**, 056105 (2012).
[16] J. Park *et al.*, Physics of Plasmas **16**, 056115 (2009).
[17] A. Turnbull, Nuclear fusion **52**, 054016 (2012).
[18] R. Moyer *et al.*, Nuclear fusion **52**, 123019 (2012).
[19] R. La Haye, Physics of Plasmas **13**, 055501 (2006).
[20] J. Scoville *et al.*, Nuclear fusion **31**, 875 (2011).
[21] B. Ayten, and E. Westerhof, Physics of Plasmas **19**, 092506 (2012).
[22] R. La Haye *et al.*, Nuclear fusion **48**, 054004 (2008).
[23] Y. Park, and A. Welander, Plasma Physics and Controlled Fusion **48**, 1447 (2006).
[24] H. van den Brand *et al.*, Nuclear fusion **53**, 013005 (2012).
[25] B. Tobias *et al.*, Review of Scientific Instruments **81**, 10D928 (2010).
[26] M. Austin, and J. Lohr, Review of Scientific Instruments **74**, 1457 (2003).
[27] R. La Haye *et al.*, Physics of Plasmas **10**, 3644 (2003).
[28] B. Tobias *et al.*, Plasma Science, IEEE Transactions on **39**, 3022 (2011).
[29] R. Fitzpatrick, Physics of Plasmas **2**, 825 (1995).
[30] J. Meskat *et al.*, Plasma Physics and Controlled Fusion **43**, 1325 (2001).
[31] I. Classen *et al.*, Physical Review Letters **98**, 35001 (2007).
[32] G. Spakman *et al.*, Nuclear fusion **48**, 115005 (2008).
[33] B. Tobias *et al.*, Review of Scientific Instruments (2012).
[34] E. de la Luna *et al.*, Review of Scientific Instruments **75**, 3831 (2004).
[35] S. Rathgeber *et al.*, Plasma Physics and Controlled Fusion **55**, 025004 (2012).
[36] W. D. D'haeseleer, *Flux coordinates and magnetic field structure: a guide to a fundamental tool of plasma structure* (Springer Series in Computational Physics, 1991).
[37] B. J. Tobias *et al.*, Physics of Plasmas **18**, 056107 (2011).
[38] T. Hender *et al.*, Nuclear fusion **44**, 788 (2004).

[39] Y. Liu *et al.*, Physics of Plasmas **7**, 3681 (2000).
[40] Y. Liu, A. Kirk, and E. Nardon, Physics of Plasmas **17**, 122502 (2010).
[41] H. Stoschus *et al.*, Journal of nuclear materials **415**, S923 (2011).

## List of Figure Captions

**Figure 1.** In (a), ECE-Imaging data (perturbed ECE radiation temperature at 29.5 kHz) is overlaid on an equilibrium reconstruction of shot 148753 at 3140 ms. Dashed contours identify the $q$ = 3/2 radius and $\varrho$ = 0.95. The coherent mode amplitude (b) and phase (c) are also shown. Mapping of the data in major radius is accomplished by evaluation of the local cold-resonant frequency of 2$^{nd}$ harmonic cyclotron oscillation, which is an acceptable mapping to real space for optically thick frequencies but should not be interpreted as physically meaningful for frequencies below the cold-resonance of the LCFS.

**Figure 2.** (a) Radially resolved FFT spectra obtained from the 1D ECE radiometer (shot #148753, t=3136 ms) are shown along with the frequency of toroidal fluid rotation (and the second harmonic thereof, white lines) as measured by CER analysis for the dominant impurity species (Carbon). A vertical dashed line identifies the inversion radius of the magnetic island chain near 2.06 m ($\varrho$=0.48). This radius is also indicated in representations of the eigenmode amplitude (b) and phase (c). The 1D radiometer observes a portion of the coherent oscillation detected at the edge of the plasma, but coverage from this diagnostic only extends to $\varrho$~0.9 for the given discharge conditions.

**Figure 3.** a) The amplitude of coherent fluctuations in electron temperature, $T_e$, in the region of the internal kink mode ($\varrho$~0.35) is shown to be correlated to the amplitude of $n$=2 oscillations measured by the poloidal Mirnov coil array. b) No such correlation with the estimated island width is observed.

**Figure 4.** a) The amplitude of the coherent $n$=2 plasma response (solid line) is plotted as a function of minor radius using combined data from all 20 ECE-Imaging lines of sight. The phase of the eigenfunction relative to the selected FFT window is plotted along the 3$^{rd}$ (triangle), 7$^{th}$ (diamond), and 11$^{th}$ (plus sign) lines of sight. These views correspond to chords near z=0, 10, and 20 cm. b) The orientation of displaced flux surfaces, as determined from this ECE-Imaging data, is illustrated. Vertical dashed lines represent the center of the island chain and the LCFS. No counter-examples to this phase relationship between the island separatrix and displaced boundary have been observed on DIII-D.

**Figure 5.** 2D ECE-Imaging data is decomposed into radially resolved poloidal basis functions, or m-numbers, and compared to the safety factor, or $q$ profile. In a) basis functions vary sinusoidally as a function of the straight-field line poloidal angle. The response at the edge is shown to be a ballooning eigenfunction with $m$-numbers dissimilar to the core response. In b), a cylindrical coordinate system is used, such that poloidal angle is the simple polar coordinate in the poloidal plane. In c), the 2D eigenfunctions represented by the poloidal mode number decomposition are plotted, along with the ECE-Imaging view, on an equilibrium reconstruction of the discharge.

## List of Figures

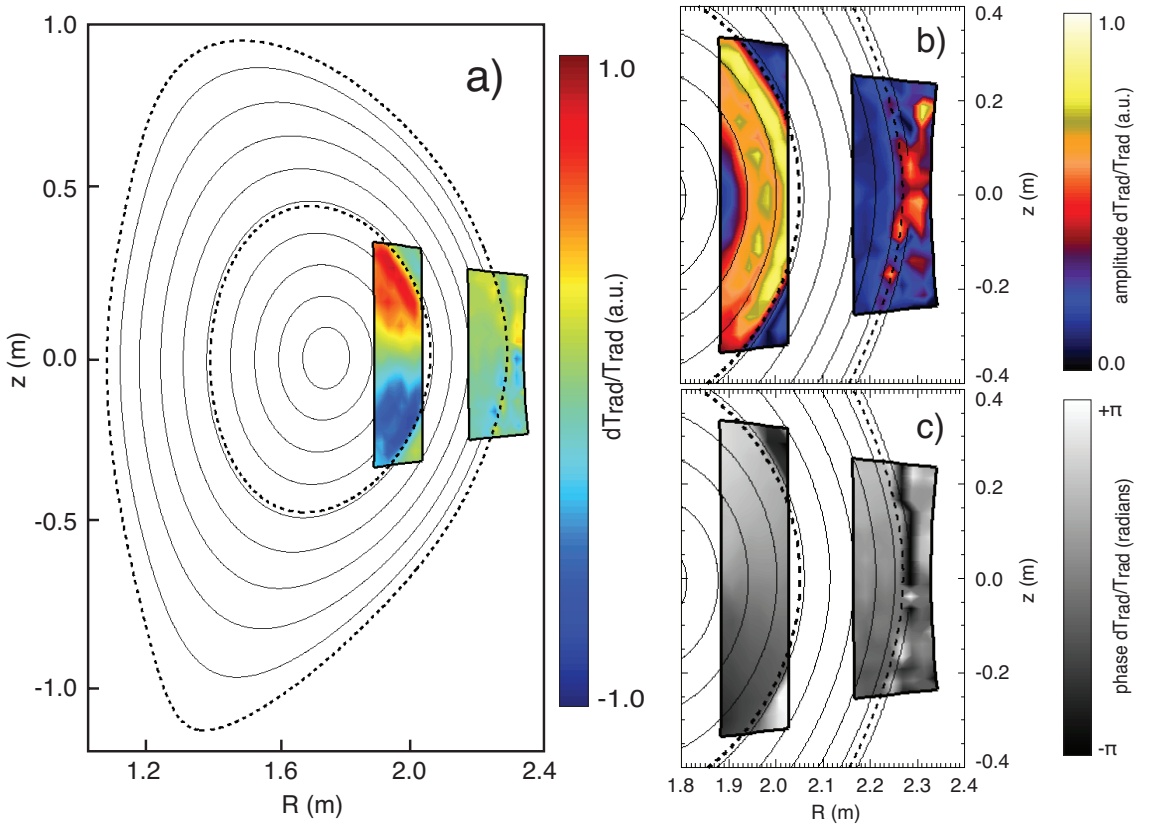


**Fig. 1**

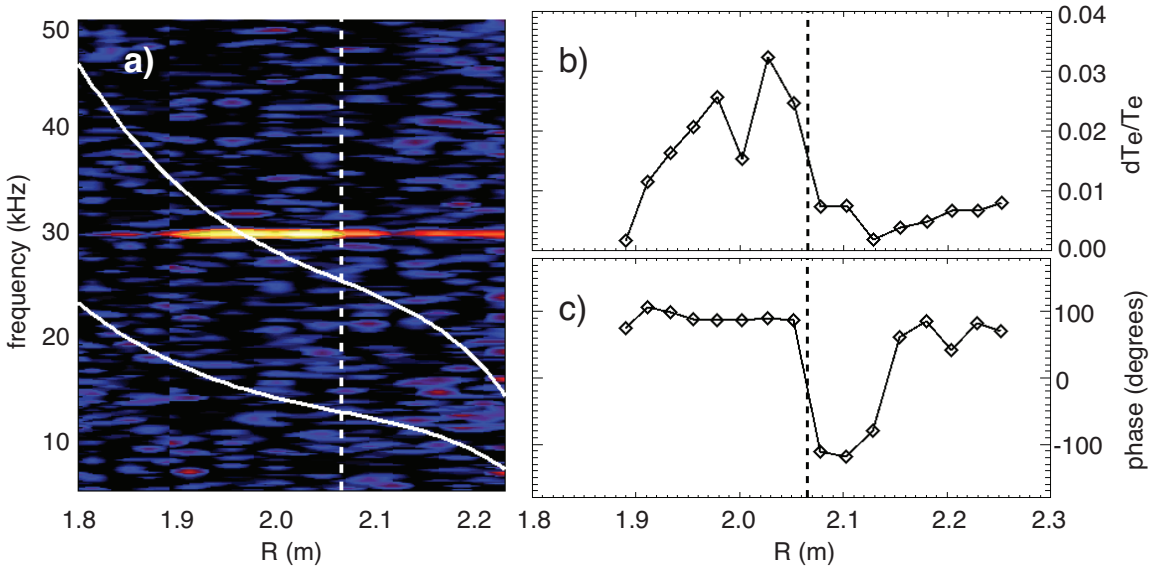


**Fig. 2**

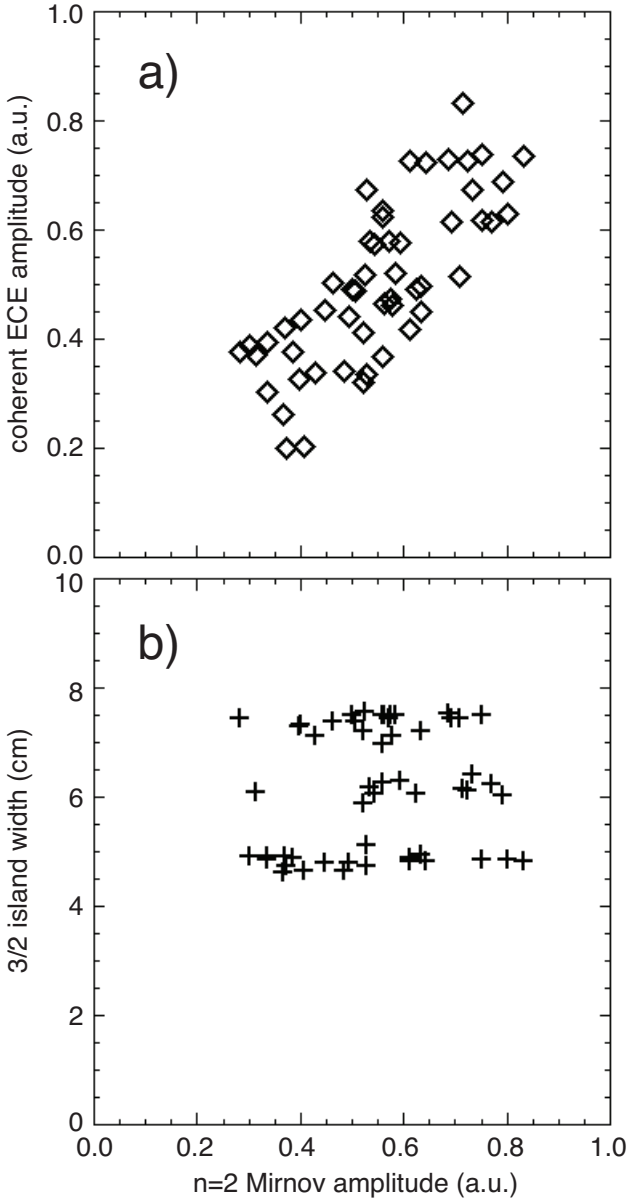
a)
b)
coherent ECE amplitude (a.u.)
3/2 island width (cm)
n=2 Mirnov amplitude (a.u.)
0.0
0.2
0.4
0.6
0.8
1.0
0
2
4
6
8
10

**Fig. 3**

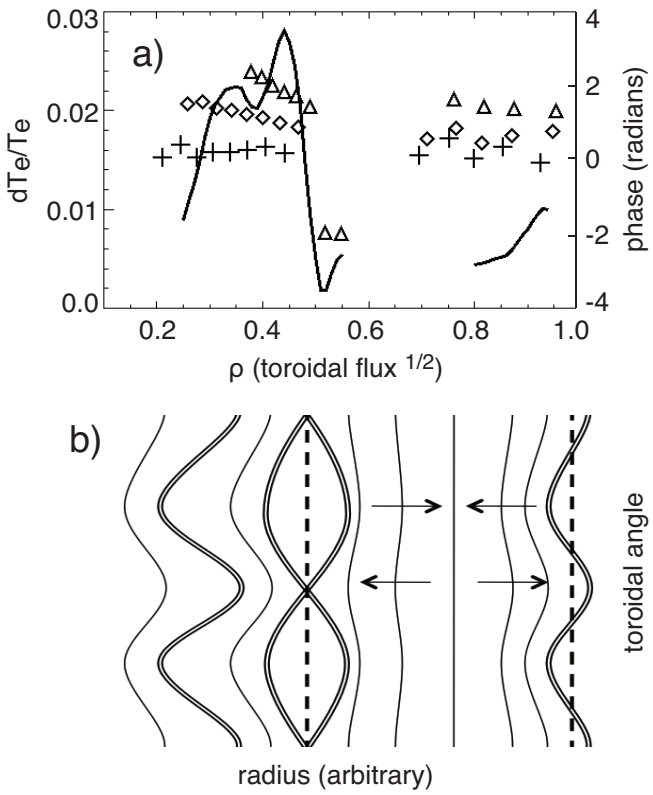
a)
dTe/Te
phase (radians)
ρ (toroidal flux 1/2)
b)
toroidal angle
radius (arbitrary)

**Fig. 4**

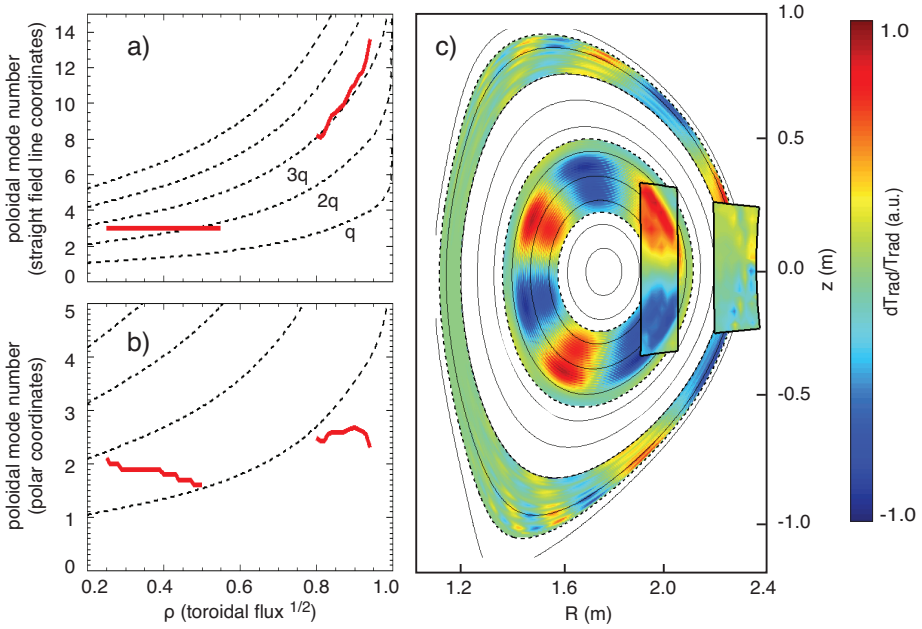
a)
poloidal mode number
(straight field line coordinates)
3q
2q
q
b)
poloidal mode number
(polar coordinates)
ρ (toroidal flux 1/2)
c)
z (m)
R (m)
dTrad/Trad (a.u.)

**Fig 5**

The Princeton Plasma Physics Laboratory is operated
by Princeton University under contract
with the U.S. Department of Energy.

Information Services
Princeton Plasma Physics Laboratory
P.O. Box 451
Princeton, NJ 08543

Phone: 609-243-2245
Fax: 609-243-2751
e-mail: pppl_info@pppl.gov
Internet Address: http://www.pppl.gov